

# DetailCLIP: Injecting Image Details into CLIP's Feature Space

Zilun Zhang<sup>\*†</sup>  
zilun.zhang@zju.edu.cn  
Zhejiang University  
Hangzhou, Zhejiang, China

Cuifeng Shen<sup>\*</sup>  
2101213250@stu.pku.edu.cn  
Peking University  
Beijing, Beijing, China

Yuan Shen  
shenyuan02@megvii.com  
Megvii Inc.  
Beijing, Beijing, China

Xinyu Zhou  
zxy@megvii.com  
Megvii Inc.  
Beijing, Beijing, China

Huixin Xiong  
xionghuixin@megvii.com  
Megvii Inc.  
Beijing, Beijing, China

Jianwei Yin  
zjuyjw@zju.edu.cn  
Zhejiang University  
Hangzhou, Zhejiang, China

## ABSTRACT

Although CLIP-like Visual Language Models provide a functional joint feature space for image and text, due to the limitation of the CLIP-like model's image input size (e.g., 224), subtle details are lost in the feature representation if we input high-resolution images (e.g., 2240). Our proposed framework addresses this issue by generating a **single feature representation** for a high-resolution image that retains image details from different scales while sharing the same semantic space as the original CLIP. To achieve this, we develop a feature fusion model that relies on CLIP features extracted from a carefully designed image patch method, dubbed Complete Cover. This method ensures comprehensive coverage of objects across various scales and is weakly supervised by image-agnostic class prompted queries. We evaluate our framework's performance using real-world and synthetic datasets, demonstrating significant improvements in image retrieval tasks based on class prompted queries. To further showcase our framework's capability in detail retrieval, we introduce a CLEVR-like synthetic dataset, named CLVER-DS. This fully annotated dataset offers a controllable object scale, allowing for a more thorough examination of our approach's effectiveness.

## CCS CONCEPTS

• **Computing methodologies** → **Image representations**; • **Information systems** → **Image search**.

## KEYWORDS

Text-Based Information Retrieval, Fine-Detail, CLIP, Single Feature, Detail Compression, Complete Cover, Feature Space Alignment, Self-Supervised

<sup>\*</sup>Both authors contributed equally to this research.  
<sup>†</sup>correspondent author

Permission to make digital or hard copies of all or part of this work for personal or classroom use is granted without fee provided that copies are not made or distributed for profit or commercial advantage and that copies bear this notice and the full citation on the first page. Copyrights for components of this work owned by others than ACM must be honored. Abstracting with credit is permitted. To copy otherwise, or republish, to post on servers or to redistribute to lists, requires prior specific permission and/or a fee. Request permissions from [permissions@acm.org](mailto:permissions@acm.org).  
31st ACM International Conference on Multimedia, 2023, Ottawa, Canada  
© 2018 Association for Computing Machinery.  
ACM ISBN 978-1-4503-XXXX-X/18/06...\$15.00  
<https://doi.org/XXXXXXXX.XXXXXXX>

## ACM Reference Format:

Zilun Zhang, Cuifeng Shen, Yuan Shen, Xinyu Zhou, Huixin Xiong, and Jianwei Yin. 2018. DetailCLIP: Injecting Image Details into CLIP's Feature Space. In *Proceedings of (31st ACM International Conference on Multimedia)*. ACM, New York, NY, USA, 14 pages. <https://doi.org/XXXXXXXX.XXXXXXX>

## 1 INTRODUCTION

The task of text-to-image retrieval involves retrieving pertinent images based on a text query, which could either describe the entire image or focus on a specific or small object within it. For example, when using CLIP to search for images containing a red helmet with "red helmet" as the text query, the top results typically showcase a large red helmet at the center of the image. However, we might also be interested in images of people wearing red helmets on a football field, where the helmets appear much smaller. Since CLIP is designed to match an entire image to a text description, it struggles to retrieve such images using only the "red helmet" query. This limitation poses a challenge when attempting to retrieve all related images in a database using a single word, as illustrated in Figure 1.

One approach to mitigating this issue involves dividing each image into smaller patches and performing the retrieval task based on the features of these patches. Nevertheless, this multi-feature method does not directly yield useful features for downstream tasks or end-to-end training. Models like Crop-CLIP [24] first detect objects in an image using a YOLOV5 detector, but the detector's capacity severely constrains model performance. For instance, when encountering objects from unseen classes, the model behaves erratically, and detail information about these objects is lost before the retrieval stage. Models such as MDETR [10], XDETR [2], and FILIP [27] have made significant improvements in detailed retrieval by retraining on multi-modal data and mining fine-grained relationships during training. However, these models require enormous training data and computational resources.

In this paper, we present a novel framework called "Detail Injected CLIP (**DetailCLIP**)" that addresses the challenges associated with text-to-image retrieval tasks at a minimal cost.

By examining the retrieval performance of CLIP-like models across various object scales, we identify the specific object scales where these models can maintain optimal performance. Leveraging this insight, we develop an image patching scheme called "Complete Cover (CC)" capable of encompassing objects of any scale. Subsequently, we employ a transformer to fuse features extracted by CLIP-like models from patches generated using the CC scheme.

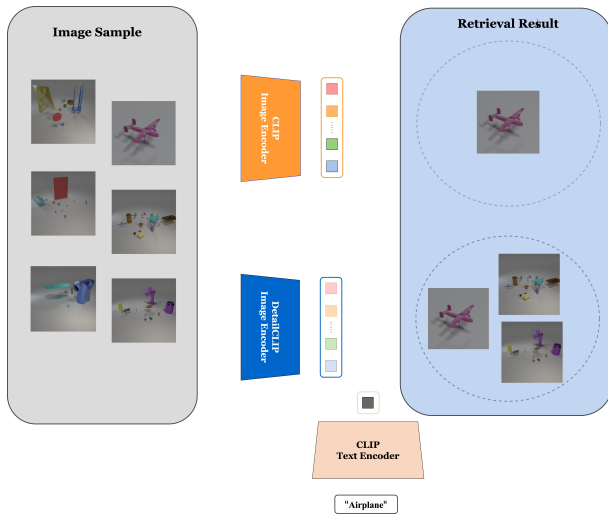


**Figure 1: Retrieval Results: CLIP Model vs. DetailCLIP Model.** The image encoder of DetailCLIP is built upon the vanilla CLIP (for more details, see Section 3.4), and both DetailCLIP and CLIP models share the same text encoder. Given a text query such as "airplane", the vanilla CLIP model can only retrieve one image with a large airplane target. In contrast, DetailCLIP successfully retrieves all three relevant images, even when the target objects are extremely small. For zoomed-in images and additional retrieval results, please refer to Appendix A.6.

Additionally, we design a self-supervised learning loss function to align detailed information with the newly fused single feature.

Our **DetailCLIP** framework enables the integration of detailed image information into a single feature that can be directly utilized for end-to-end training, requiring only the cost of training a small transformer. Our main contributions can be summarized as follows:

- Focusing on the detailed class-with-prompt text-to-image retrieval task and proposing **DetailCLIP**, an efficient framework capable of generating a single image feature containing detailed information. We evaluate our framework on MSCOCO, LVIS, and synthetic datasets, demonstrating superior performance compared to existing vision-language models. Moreover, our framework can also be used as a **plug-in module**, which could improve the ability of retaining detail information in the extracted feature **for other Vision-Language Models** in general.
- Introducing a novel image patching scheme called "Complete Cover (CC)" that can theoretically cover objects of any scale while minimizing redundant patches.
- Developing a retrieval benchmark based on CLEVR [9] and ShapeNet [3] 3D objects called "CLEVR of Different Scales (CLEVR-DS)". This fully annotated and object scale-controllable dataset demonstrates that our framework significantly outperforms current methods in retrieval performance.

The remainder of this paper is organized as follows: Section 2 discusses related works; Section 3 provides a detailed description of

our proposed "Complete Cover (CC)" method and the **DetailCLIP** framework with corresponding loss; Section 4 introduces our proposed benchmark; and Section 5 presents experiments that validate the superiority of our framework.

## 2 RELATED WORK

### 2.1 Overview of Vision-Language Models

Current Vision-Language Models can be classified based on their task objectives. Models such as CLIP [20], ALIGN [8], and Flamingo [1] align textual and visual information into a shared semantic space using contrastive learning tasks. VisualBERT [14], UNITER [4], and DALL-E [21] focus on region modeling or text-guided image generation. Single-stream models like VisualBERT and ViLT [11] concatenate visual and textual features and feed them into a unified encoder-like transformer. Dual-stream models, including CLIP, FILIP [27], and ViLBERT, have separate encoders for different modalities. Other models cater to specific tasks, such as MDETR [10] for object detection, PhraseCut [25] for segmentation, and Florence [28] for foundation models.

### 2.2 CLIP-like Models

CLIP [20] is a neural network developed by OpenAI, trained on various image-text pairs. Given an image, CLIP predicts the most relevant text snippet or vice versa. CLIP's zero-shot performance on the ImageNet classification task is comparable to that of the original ResNet50, akin to GPT-2 and GPT-3's zero-shot capabilities, and is robust to Natural Distribution Shift [6]. However, CLIP features have limitations, such as susceptibility to typographic attacks or fine-grained concepts. Additionally, [30] posits that text feature quality is highly related to prompt methods (ways to augment class labels to generate text sentences). In SLIP [18], different views of each input image are used for text supervision and image self-supervision, illustrating that image self-supervision benefits CLIP's performance. Concurrently, DeCLIP [16] adds several additional training objectives to CLIP to enhance language supervision. Recently, GLIP [15] was proposed, unifying object detection and phrase grounding for pre-training and learning object-level, language-aware, and semantically rich visual representations.

### 2.3 Applications of Vision-Language Models

MDETR [10], a modulated detector for multi-modal understanding, has achieved state-of-the-art results on multiple datasets. However, its use of an expensive modal joint transformer to align language and vision makes it impractical for real-world applications. XDETR [2] aligns an object's bounding box with free-form language instead of the entire image. Its architecture comprises three main components: object detector, language encoder, and alignment. Visual and linguistic data streams remain independent until the end and are aligned using dot product operations. XDETR demonstrates high accuracy and speed in multi-instance multi-modal tasks (e.g., 16.4 AP on LVIS detection of 1.2K categories).

To capture fine-grained alignment between images and text, RegionCLIP [29] creates a pool of object concepts from the text corpus and employs a pre-trained CLIP model to align a concept with an image region, generating pseudo labels. They use region-text pairs and ground-truth image-text pairs to pretrain a vision-language

**Table 1: Performance of CLIP text-image retrieval task with different LVIS subsets.**

$r_{max}$	Recall@1	Recall@3	Recall@5
$10^0$	8.63%	15.19%	18.60%
$10^{-0.5}$	7.52%	13.87%	17.45 %
$10^{-1}$	5.75%	11.28%	14.66 %
$10^{-1.5}$	4.92%	9.61%	12.16 %
$10^{-2}$	3.98%	8.76%	11.48 %

Refer to section 4.3 for the metric detail

model. RegionCLIP exhibits a superior ability to recognize region objects and successfully transfers to the open-vocabulary object detection task, although it lacks an analysis of small object detection in images. GroupViT [26] incorporates a grouping mechanism into deep networks, enabling semantic segments to emerge automatically with only text supervision. It learns to group semantic regions together and successfully transfers to the semantic segmentation task.

### 3 METHODOLOGY

#### 3.1 Motivation and Effective Scale Sensitivity

CLIP’s ability to retrieve objects declines as the object’s size decreases. We conduct our experiment on the LVIS dataset [7] and use

$$r_{max} = \frac{\text{Maximum Area of the Objects in the image}}{\text{Area of the Image}} \quad (1)$$

with varying values as an upper bound (threshold) to create subsets of LVIS. We choose LVIS because it contains more categories than COCO [17] and includes more annotations for small objects. As demonstrated in Table 1, CLIP’s performance consistently decreases as object size diminishes.

We define the Effective Scale Sensitivity of CLIP-like models as the minimum object occupying percentage in an image that CLIP-like models can retrieve. We need to input images within the sensitivity of CLIP-like models. A natural thought in solving this problem is slicing an image into small patches and retrieving objects on those patches. Consider the side length of an image is  $n$ , and the number of possible patches to cover all possible objects is  $O(n^4)$  level which is unbearable. We propose the "Complete Cover (CC)" method to eliminate redundant patches while covering all possible objects.

#### 3.2 Problem Definition

In this section, we provide a formal problem definition for Detail Injection using CLIP-like models, an image, and a set of image patches. Suppose we generate  $p$  patches from an image  $X$ , and we denote the set of image patches as  $x_i \in X$ , where  $i \in 1, \dots, p$ . Then,  $\mathcal{F} : \mathbb{R}^{c \times w \times h} \rightarrow \mathbb{R}^d$  represents the CLIP-like models’ image encoder, and the  $d$ -dimensional feature  $u_i$  extracted from a single image patch  $x_i$  can be expressed as:

$$u_i = \mathcal{F}(x_i), \quad (2)$$

We denote the set of image patch features for a given image as  $U = \{u_i\}$ , where  $i \in \{1, \dots, p\}$ . We define our fusing model as  $\mathcal{D} : \mathbb{R}^{p \times d} \rightarrow \mathbb{R}^d$ . The DetailCLIP feature  $v$  is obtained from:

$$v = \mathcal{D}(U), \text{ where } v \in \mathbb{R}^d \quad (3)$$

#### 3.3 Complete Cover

In this subsection, we introduce a patch generation scheme. Given an image with a side length of  $n$ , the complexity of the number of possible patches needed to cover all objects is on the order of  $O(n^4)$ , which is computationally infeasible. To address this issue, we propose the "Complete Cover (CC)" method, which aims to eliminate redundant patches while ensuring complete coverage of all possible objects. A schematic representation of the **Complete Cover** method can be found in Figure 2.

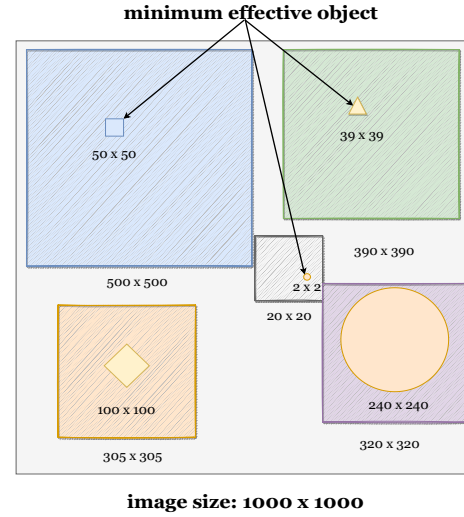


**Figure 2: Illustration of Patch Selection of Complete Cover. Minimum effective object means the minimum object that can be retrieved by CLIP from the patch. Patches with different shapes will slide the whole image to cover objects equal to or bigger than the minimum effective size.**

First, we define the concept of **cover**. Let  $Q$  represent the set of pixels in a patch, and  $P$  denote the set of pixels within an object’s bounding box. In order to ensure that the patch includes objects while retaining its retrieval capability, we define  $Q$  covers  $P$  as follows:

$$Q \text{ covers } P := C(Q, P) = \begin{cases} \text{True,} & \forall p = (x, y) \in P \rightarrow p \in Q \text{ and } |P| > c^2 \cdot |Q| \\ \text{False,} & \text{Otherwise} \end{cases}$$

where  $|\cdot|$  is the number of pixels in  $\cdot$ .

and  $c$  is effective scale sensitivity defined in our paper (4)

Next, we define the set of all possible  $P$  in an image as  $S_{\text{full}}$ . In the "Complete Cover (CC)" scheme, we design a greedy algorithm to generate a set of  $Q$  as  $S_{\text{cc}}$ , which fulfills:

$$\forall P \in S_{\text{full}}, \exists Q \in S_{\text{cc}}, s.t. C(Q, P) = 1 \quad (5)$$

The specific patch selection method is as follows: Given an effective scale sensitivity  $c$ , assume the full image pixel set is  $Q_0 \in S_{\text{cc}}$ , all the objects bounding box pixel set  $P_0 \in S_{\text{full}}$  it can cover satisfies:

The specific patch selection method proceeds as follows: Given an effective scale sensitivity  $c$ , assume the full image pixel set is  $Q_0 \in S_{\text{cc}}$ , and all object bounding box pixel sets  $P_0 \in S_{\text{full}}$  that it can cover satisfy:

$$C(Q_0, P_0) = 1, \forall P_0 \in S_{\text{full}}, \text{if } |P_0| > c^2 \cdot |Q_0|, \quad (6)$$

Without loss of generality, let  $P \in S_{\text{full}}$  be square and  $P_0$  have a side length of  $a$ . In order to cover  $P_1 \in S_{\text{full}}$  with a side length of  $a/c - 1$ , we employ a greedy approach to obtain  $Q_1 \in S_{\text{cc}}$  such that  $C(Q_1, P_1) = 1$ . This is achieved by passing a global sliding window with a side length of  $a - c$  and a step size of  $a/c - 2$ . We repeat this procedure until we have patches that can cover objects with side lengths ranging from  $a/c$  to  $a/c - n$ , where  $n = a/c - 1$ . The complexity of the number of possible patches needed to cover all objects reduces from  $O(n^4)$  to  $O(n^2)$ , a proof can be found in Appendix A.1.

Our CC method can better retain detailed information compared to simply slicing the image into non-overlapping, equal-sized patches as proposed by [5]. CC faces a trade-off between completeness and computational complexity with different values of  $c$ . A reasonable choice of  $c$  should generate a manageable number of patches while ensuring the preservation of detailed information.

### 3.4 Model & Loss

In this subsection, we propose a fusion model and a proxy loss. Assuming the patch selection method is determined, we extract features from each image patch and use CLIP prompts to convert all class labels into sentences, extracting features for each sentence. This section focuses on fusing multiple patch features into a single feature and utilizing the image-agnostic text feature as a proxy for injecting detailed information. The framework's overview architecture is depicted in Figure 3.

**3.4.1 Fusing Model.** The core principle of DetailCLIP is to combine features from different patches into a single new feature while preserving as much detail as possible. There are numerous options for implementing the fusing model, such as learning a weight to average patch features, using a linear projection, or employing an MLP. We opt to implement the fusing model with a small transformer. Specifically, the input for this fusing model consists of two components: features for all patches and the feature for the entire image. We use the former as the input source and the latter as the input target in the transformer.

**3.4.2 Query Proxy Loss.** In the context of small objects within an image, there will be one patch feature containing the most information about the object, which we denote as  $u_{\text{max}} \in U$ . The loss function aims to inject the patch feature information which contains the most detailed information about the small object, into the fused

feature. Specifically, we use a text feature  $w$  that describes the small object in the image as a proxy feature to draw the fused feature  $v$  closer to the patch feature  $u_{\text{max}}$ . This is because the text feature resides in the same joint feature space as the image feature. We use a similarity function to measure the similarity between the proxy feature and the candidate patch feature, selecting the most similar patch feature as  $u_{\text{max}}$ . Simultaneously, we calculate similarities between the fused feature and the proxy feature. Then, we minimize the distance function to bring these two similar distributions closer together.

$$L_{\text{qp}} = D[\text{sim}(v, w), \text{sim}(w, u_{\text{max}})] \quad (7)$$

where  $w \in \mathbb{R}^d$  has the same dimension as  $v$  and  $u_{\text{max}}$ . The symbol  $\text{sim}$  represents the similarity measure function, while the symbol  $D$  denotes the distance measure function. We aim to learn  $v$  such that the distance between the similarity distribution of  $v$  and  $w$  and the similarity distribution of  $u_{\text{max}}$  and  $w$  is minimized. For every batch of images, we use all class-prompted text features to calculate similarity, without requiring additional supervision beyond the class name in the dataset.

A PyTorch style code and the complete pipeline of our model can be seen at Appendix A.5.

## 4 BENCHMARK

In text-image retrieval, the traditional task of "using a caption to retrieve a single image" is widely employed to evaluate a model's retrieval capability. However, the practical requirement of "using a word to retrieve all related images in a database" remains unaddressed. Traditional text-image retrieval datasets like Flickr30k and COCO-caption (MSCOCO dataset utilizing captions for retrieval) are not suitable for evaluating the latter task. We select some object detection datasets and use "prompting with class name" as a text query to retrieve all related images in a database. We construct the benchmark for this vital task by adopting existing datasets, making a new synthetic dataset, and designing the evaluation metrics.

### 4.1 Existing Datasets

In theory, numerous existing datasets with class-wise object supervision and class names can be utilized to construct the benchmark. However, both have deficits not only for the proposed task but also for analyzing methods' detail retrieval capabilities. Examples are displayed in Figure 4.

For real-world datasets, the label information in Visual Genome [12], ImageNet-1K [22], and GPR1200 [23] primarily focuses on the main object in the image. As these datasets are sourced from real-world scenes, achieving complete-annotation of the images is challenging, resulting in insufficient fine-detail annotation. Furthermore, the large dataset LVIS [7] contains many missing labels, making it impossible to draw accurate conclusions during retrieval evaluation. Synthetic datasets such as CLEVR by [9] and SHOP-VRB by [19] have too few object categories. Additionally, these datasets lack specific design considerations for object size in the images.

### 4.2 CLEVR-DS

**4.2.1 Summary of CLEVR-DS.** To achieve accurate retrieval evaluation, we created a dataset called "CLEVR of Different Scales

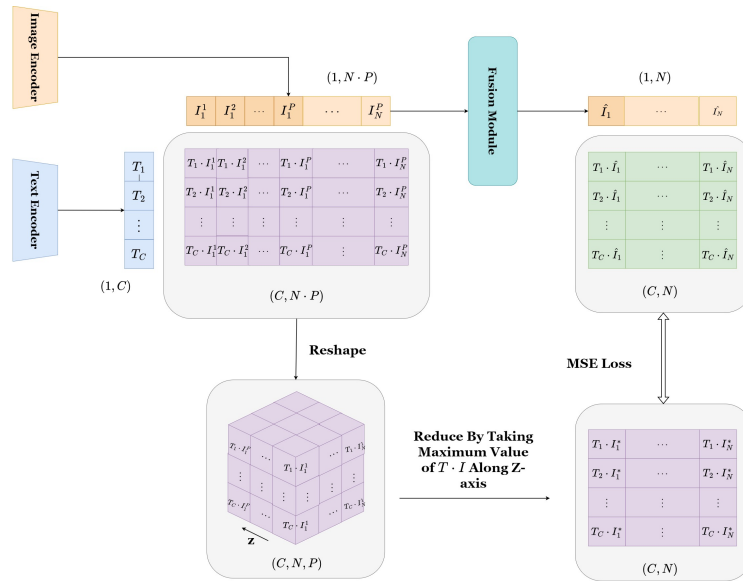


Figure 3: The DetailCLIP framework with feature query proxy loss is illustrated in the figure. Here,  $N$  represents the number of images,  $P$  is the number of patches per image, and  $C$  is the number of classes in a given dataset.  $I$  and  $T$  correspond to the image and text features, respectively. For instance,  $I_2^2$  denotes the  $2^{nd}$  patch of the  $1^{st}$  image, while  $T_1$  refers to the text feature for class 1. The framework consists of two branches for patch-wise image features. In the first branch, patch-wise image features are merged into image-wise features using the fusing module (in Tiffany Blue) to obtain detail-enhanced image features. The cosine similarity between text features and image-wise features is then calculated (in green). In the second branch, patch-wise image features are used to compute the cosine similarity with the text features, respectively. The maximum similarity value over different patches within the same image is selected to represent the image-wise cosine similarity to the text (bottom-right corner). Finally, the query proxy loss is computed using the similarity distributions from two branches.

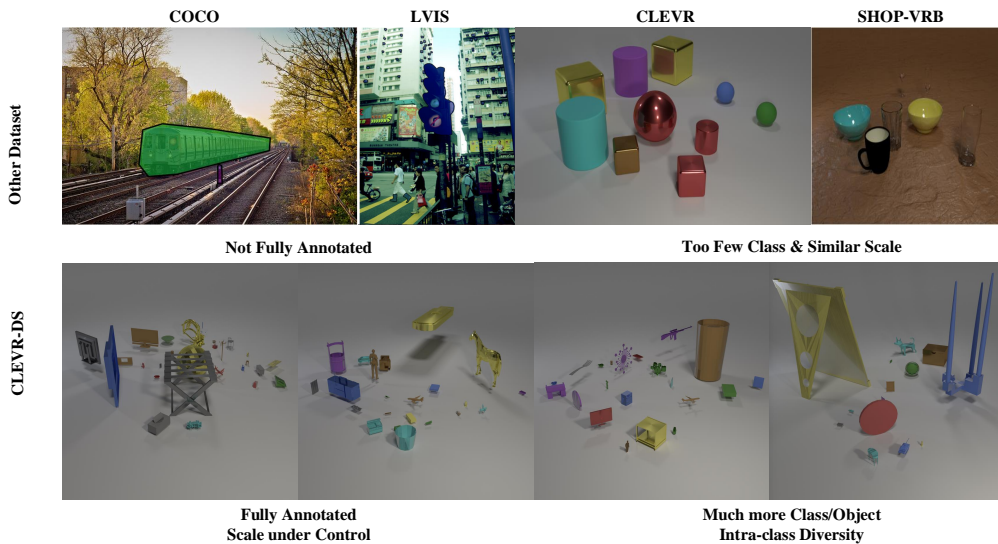


Figure 4: Illustration for different datasets. Existing datasets have different flaws for the retrieval by classname task. COCO and LVIS are not fully annotated, while CLEVR and SHOP-VRB, though fully annotated, have a limited number of classes and monotonous object scales. In contrast, our proposed CLEVR-DS dataset is fully annotated for retrieval tasks and features a greater variety of classes and objects with different scales, thereby increasing intra-class diversity.

(CLEVR-DS)," which includes 138 categories from ShapeNet and has an average of nearly 14 instances per image, surpassing LVIS. This dataset allows for complete-annotation information (e.g., spatial position, bounding box, category, and attribute) in the image. Our CLEVR-DS covers a wide range of object scales (small, medium, and large) and exhibits greater variability in scene complexity. Additional statistics and visualizations of the CLEVR-DS dataset can be found in Appendix A.2.

### 4.3 Evaluation Metrics

The current evaluation metric for text-to-image retrieval calculates the top  $k$  recall accuracy of a text query. However, as we focus on retrieving all related images in a database, the top  $k$  retrieval result is insufficient for evaluating our method's performance. We propose a new evaluation metric, Recall@ $k$ , to assess retrieval performance. Recall@ $k$  is calculated as follows:

$$\text{Recall}@k = \frac{t_k}{n} \quad (8)$$

where  $n$  is the number of images of the query (also a class) in the database.  $t_k$  represents the number of images containing the query in the first  $n \times k$  retrieved images.

For the number  $k$ , we select 1, 3, and 5 as the anchor points for evaluation indicators. All datasets are assessed using this method.

## 5 EXPERIMENTS

### 5.1 Implementation Details

**Dataset setting:** Our primary focus is on two types of datasets: synthetic and real-world datasets. As synthetic datasets are completely annotated, we test our model's image fine-detail retrieval ability by setting the size of objects in the image. For CLEVR-DS, we define two sub-datasets: CLEVR-DS-S and CLEVR-DS-L, which contain only small or large objects of the query semantic information, respectively, as well as the distractor data. For Unity-Retail datasets, we randomly split them into a 7:1:2 ratio for training, validation, and test sets.

We also evaluate our model on real-world datasets, such as MSCOCO and LVIS. For MSCOCO, we randomly select 5000 images for validation and use the original validation set for testing. Since LVIS shares the same images as MSCOCO, we apply the same split setting as MSCOCO.

**Model architecture:** We utilize three types of CLIP-like image and text encoders; the first two are implemented by [18], which use ViT-B/16 as their backbone, and the third is presented by [20], which employs ViT-L/14 as its backbone. To test the generalizability of the DetailCLIP framework, we use CLIP-like models as image encoders to extract features. Additionally, image and text features are mapped into 512 and 768 dimensions for different image encoder architectures. We employ a small transformer structure for the image feature fusing model with three encoders and three decoders. The entire framework is optimized using query proxy loss.

**Patch selection mode:** In the main results, we use CC to represent the patch selection method. To save computational resources, we set the number of patches to 166 (cc@10). We evaluate the CLIP-like model's retrieval ability for untrained retrieval using both the CC patches and whole image features. Specifically, we select the

**Table 2: Retrieval Performance of DetailCLIP and CLIP on CLEVR-DS.**

Dataset	Method	Single Feature	Input	Recall@1	Recall@3	Recall@5
CLEVR-DS	CLIP	✓	Full Image	10.61%	29.64%	49.50%
	CLIP	×	CC@10	<b>22.56%</b>	45.45%	64.91%
	<b>DetailCLIP</b>	✓	CC@10	22.54%	<b>46.16%</b>	<b>64.98%</b>
CLEVR-DS-S	CLIP	✓	Full Image	4.43%	16.25%	30.32%
	CLIP	×	CC@10	14.57%	32.55%	<b>37.12%</b>
	<b>DetailCLIP</b>	×	CC@10	<b>14.66%</b>	<b>32.77%</b>	32.78%
CLEVR-DS-L	CLIP	✓	Full Image	13.57%	23.19%	28.65%
	CLIP	×	CC@10	15.30%	<b>25.93%</b>	<b>31.97%</b>
	<b>DetailCLIP</b>	✓	CC@10	<b>16.33%</b>	25.47%	30.96%

highest CC patch score as the image retrieval score. For CC@ $\cdot$ , the  $\cdot$  represents the selection of the hyper-parameter effective scale sensitivity. In the DetailCLIP scenario, the CC patch features are utilized to train the model. An analysis of selecting the value of  $k$  can be found in Appendix A.3.

**Training Details:** Details for hyperparameter search are listed in Appendix A.4.

### 5.2 Main Result Analysis

Before analyzing the retrieval performance, we would like to clarify a point. For the cc@10 input type, "single feature" refers to using a single image feature vector to represent the image and performing the retrieval task based on it. In this case, details from all patches are merged and injected into a single vector. On the other hand, cc@10 input with "non-single features" indicates the use of multiple image feature vectors (one for each patch), which is computationally expensive (refer to the ablation study later) and inconvenient for end-to-end retrieval tasks or other downstream tasks that require a single feature. Theoretically, the cc@10 input contains an equal amount of detail information, whether it employs a single feature or multiple features. As a result, CLIP with cc@10 (multiple features) should not only serve as a baseline but also be comparable to DetailCLIP with cc@10 input in terms of retrieval performance.

**5.2.1 Results on CLEVR-DS.** We use CLIP with a ViT-B/32 backbone as the image and text feature extractor. We employ a tiny transformer with three encoders and three decoders to fuse the patch features. In the non-training scenario, we utilize single-feature and multi-feature to retrieve. The former leverages the similarity between the whole image feature and the text feature for decision-making, while the latter relies on the largest similarity between all patch features and the text feature. As demonstrated in Table 2, DetailCLIP improves the retrieval performance from 10.61% to 22.54% on the CLEVR-DS dataset, with mixed object size. In the meanwhile, DetailCLIP significantly enhances performance on the CLEVR-DS-S subset by 10.23% and shows a reasonable improvement in the CLEVR-DS-L subset by 2.76%.

**5.2.2 Results on Real-World and synthetic dataset.** We use several feature extractors to assess the performance of our DetailCLIP framework. Besides CLIP models with different size of ViT backbone (ViT-B/16 and ViT-L/14), various models are compared as well. Specifically, we select a region-based approach, RegionCLIP (utilize a detector to propose region); a CLIP variant approach, SLIP (CLIP

**Table 3: Retrieval Performance of DetailCLIP framework and other methods on four datasets.**

DATASET			LVIS	COCO	Unity	CLEVR-DS
Method	Single Feature	Input	Recall@1	Recall@1	Recall@1	Recall@1
§ CLIP-ViT-B/16	✓	Full Image	7.49%	40.93%	24.63%	8.51%
§ CLIP-ViT-B/16	×	CC@10	<b>9.40%</b>	41.24%	23.11%	17.03%
<b>DetailCLIP</b>	✓	CC@10	7.66%	<b>44.19%</b>	<b>25.02%</b>	<b>18.09%</b>
† CLIP-ViT-L/14	✓	Full Image	15.12%	56.74%	35.74%	13.81%
† CLIP-ViT-L/14	×	CC@10	<b>22.00%</b>	59.40%	52.40%	33.21%
<b>DetailCLIP</b>	✓	CC@10	15.29%	<b>62.63%</b>	<b>55.21%</b>	<b>33.46%</b>
§ SLIP	✓	Full Image	9.65%	47.49%	24.42%	9.51%
‡ RegionCLIP	✓	Full Image	10.13%	46.06%	24.10%	10.98%
BLIP2	✓	Full Image	13.36%	47.85%	32.34%	17.14%

§ Trained on YFCC-15M

† Trained on 400M images-text pairs

‡ Trained on Conceptual Caption (CC3M)

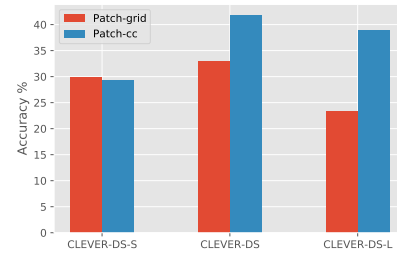
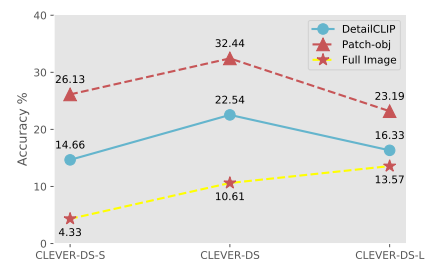
with additional self-supervised loss.); a sota approach for Vision-Language retrieval, BLIP2 [13] (ViT-G backbone). To confirm the effectiveness of our method on datasets with complex scenes, we test on the MSCOCO, LVIS, and Unity-Retail datasets. The former two are real-world datasets but lack full annotation. The latter is a synthetic dataset with more complex scenes and is fully annotated. Table 3 reveals that DetailCLIP’s retrieval results on most datasets surpass the full image baseline and CC@10 baseline. For example, on MSCOCO, DetailCLIP outperforms the full image baseline by ~ 6% in recall@1, indicating that the DetailCLIP feature performs better than the original CLIP feature in the retrieval task on the target domain. However, the margin between the full image baseline and DetailCLIP on MSCOCO (~ 6%) is smaller than on Unity-Retail (~17 %) and CLEVR-DS (~20 %). Although Unity-Retail is still a synthetic dataset, it presents more complex scenes than CLEVR-DS. We speculate that the gap in margin for different datasets is caused by the fully annotated or not fully annotated issue. For the MSCOCO dataset, DetailCLIP demonstrates performance close to selective approaches, including the sota method. In the case of the CLEVR-DS dataset, DetailCLIP outperforms all compared approaches, even surpassing the sota method. Further investigation into using DetailCLIP as a plug-in module (such as DetailSLIP, DetailBLIP, etc.) can be found in the Appendix.

## 6 ABLATION STUDY

We conduct ablation analysis on our framework, data sources, and retrieval methods to further showcase the effectiveness of the method proposed in the paper and its components. In all ablation experiments, we use CLIP-ViT-B/32 as the default feature extractor.

### 6.1 Patch Generation and Upper Bound Ablation

First, we define two patch generation schemes, "Patch-cc" and "Patch-grid." "Patch-grid" simply divides the image into non-overlapping, equal-sized patches. "Patch-cc" generates patches for an image following the Complete Cover (CC) scheme. To verify that CC can effectively generate patches with varying levels of detail for injection and fusion, we compare these two patch generation schemes on the CLEVR-DS dataset. As shown in Figure 5, patch-cc outperforms the patch-grid scheme on all sizes of CLEVR-DS datasets, except for

**Figure 5: Retrieval performance under different patch scheme****Figure 6: Retrieval result of different approach.**

CLEVR-DS-S. These results demonstrate that our patch-cc method generates superior patches compared to the patch-grid approach.

Second, the "Patch-obj" method generates patches by cropping objects from the image using their bounding boxes. We use the "Patch-obj" method to generate bounding box patches and select the one most similar to the target as the retrieval result to test the upper bound of CLIP’s retrieval ability. Intuitively, directly retrieving from bounding box patches represents the best possible performance of CLIP. In Figure 6, "Full image" refers to the retrieval using the original image CLIP feature, while "DetailCLIP" denotes the retrieval using the DetailCLIP image feature. The result of DetailCLIP with CC input, at 22.54%, is closer to the result of "Patch-obj" (32.44%). Additional ablation studies can be found in Appendix A.3.

### 6.2 Fine-tune On Target Domain

Since our method has been trained on the target dataset in an unsupervised manner, to evaluate the method’s effectiveness, we experiment with four different adaptation methods on the CLEVR-DS dataset. Each adds a trainable module on top of the CLIP model, similar to our method. We tested two types of module, MLP and Transformer, which use the original CLIP feature as input and the adapted feature on the target domain as output. Results in Table 4 show that the vanilla adaptation on the target dataset is not as effective as our method.

**Table 4: Add the trainable modules on top of the CLIP model to fine-tune**

Module		Patch-cc	Recall@1
Transformer	# of MLP-layers		
×	0	×	10.61%
×	1	×	15.91%
×	2	×	14.70%
×	3	×	13.96%
✓	×	×	15.90%
×	3	✓	17.21%
×	1	✓	17.51%
✓	×	✓	<b>22.54%</b>

### 6.3 Ablation on different object numbers

The number of instances and categories in the evaluation dataset is crucial to the performance of the image retrieval method. As shown in Table 5, we tested our method on a dataset with fewer instances per image and fewer categories. The results show that our method achieves better performance with fewer objects in an image.

**Table 5: Retrieval Performance of DetailCLIP and CLIP on CLEVR-DS with different object numbers.**

Dataset	categories	instance per image	Recall@1	Recall@5
CLEVR-DS	138	14	41.10%	73.41%
CLEVR-DS	51	3	15.30%	31.97%

### 6.4 Computational Resource Analysis

As demonstrated in Table 6, the inference time has been reduced from 4.3s to 1.3s, which is a reduction of around 70%. This significant improvement can potentially increase the speed of processing data, making retrieval tasks more efficient and responsive. Faster inference time can also lead to an improved user experience, especially in real-time scenarios where speed is critical.

Additionally, the reduction in memory usage from 333KB to 2.2KB is impressive. This represents a reduction of over 99%, which can be crucial for image retrieval tasks with limited resources. Lower memory usage means that the system can run on lower-end devices, which can result in cost savings for the hardware used to run the system.

**Table 6: Computational Resource**

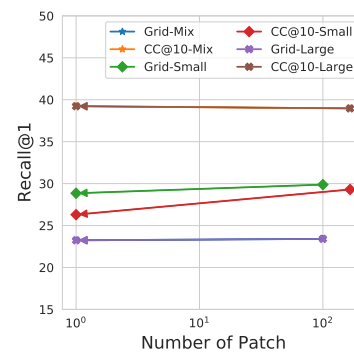
Method	patches	time(ms)	Memory(KB)	Recall@1
CC	166	4.9	333	14.66%
<b>Detailclip</b>	<b>1</b>	<b>1.3</b>	<b>2.2</b>	<b>14.57%</b>

### 6.5 Information Injection Ablation

We test the ability of the DetailCLIP framework to inject detailed information using a varying number of patches. The CLEVR-DS

dataset is used for the task. We train the DetailCLIP fusing model with different numbers of patches and test the retrieval performance of the fused feature. In Figure 7, "Grid" and "CC" represent the patch selection methods, while "Mix," "Small," and "Large" indicate the object scale in the CLEVR-DS dataset.

As shown in Figure 7, DetailCLIP's performance remains stable as the number of patches increases, demonstrating that our framework can effectively inject detailed information from multiple patches. The results also indicate that the patch generation method, whether patch-cc or patch-grid, yields similar results for DetailCLIP, comparable to the multi-feature CLIP results. This further proves that DetailCLIP can effectively inject information from various sources.

**Figure 7: After applying DetailCLIP, we achieve 100x #Patch Reduction with no significant performance loss.**

### 6.6 Similarity Distribution of Retrieval Results

We also examine the similarity distribution of positive and negative text-image pairs in Figure 8. The similarity x-axis is in log-scale, and the vertical dashed lines represent the log-scale mean of the distribution. The positive pair distribution for DetailCLIP leans more to the right than for CLIP, indicating a higher similarity between relevant text-image pairs. The log-scale distribution appears to form a normal distribution shape, which can be attributed to the fact that similarity is calculated as a normalized dot-product between text and image features. Under mild assumptions, this naturally leads to a log-normal distribution.

## 7 CONCLUSION & FUTURE WORK

In conclusion, we present DetailCLIP, a detail injected feature fusion framework designed for text-to-image retrieval tasks. DetailCLIP operates in the same semantic space as CLIP-like models and demonstrates outstanding performance in detail retrieval. We propose a Complete Cover (CC) patch selection scheme and a Transformer-based framework with query proxy loss to obtain a detail-friendly feature representation. To evaluate the retrieval performance of DetailCLIP, we constructed the CLEVR-DS dataset. Our extensive experiments on this dataset and other popular datasets show that DetailCLIP surpasses the retrieval performance of CLIP-like models. Moreover, our framework can be used as a plug-in module for



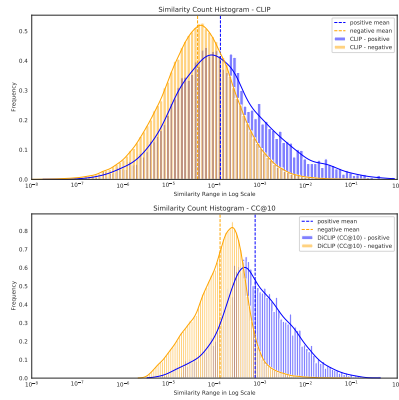


**Figure 8: Distribution of retrieval results for positive & negative samples.**

any Vision-Language Model, and improve their ability for detail retrieval. CLIP model provides a powerful semantic space, and directly removing redundant information in this space by modifying the CLIP feature could be an interesting direction for future research.

## REFERENCES

- [1] Jean-Baptiste Alayrac, Jeff Donahue, Pauline Luc, Antoine Miech, Iain Barr, Yana Hasson, Karel Lenc, Arthur Mensch, Katie Millican, Malcolm Reynolds, et al. 2022. Flamingo: a Visual Language Model for Few-Shot Learning. *arXiv preprint arXiv:2204.14198* (2022).
- [2] Zhaowei Cai, Gukyeon Kwon, Avinash Ravichandran, Erhan Bas, Zhuowen Tu, Rahul Bhotika, and Stefano Soatto. 2022. X-DETR: A Versatile Architecture for Instance-wise Vision-Language Tasks. *arXiv preprint arXiv:2204.05626* (2022).
- [3] Angel X. Chang, Thomas Funkhouser, Leonidas Guibas, Pat Hanrahan, Qixing Huang, Zimo Li, Silvio Savarese, Manolis Savva, Shuran Song, Hao Su, Jianxiong Xiao, Li Yi, and Fisher Yu. 2015. *ShapeNet: An Information-Rich 3D Model Repository*. Technical Report arXiv:1512.03012 [cs.GR]. Stanford University – Princeton University – Toyota Technological Institute at Chicago.
- [4] Yen-Chun Chen, Linjie Li, Licheng Yu, Ahmed El Kholy, Faisal Ahmed, Zhe Gan, Yu Cheng, and Jingjing Liu. [n. d.]. UNITER: UNiversal Image-Text Representation Learning. ([n. d.]). arXiv:1909.11740 <http://arxiv.org/abs/1909.11740>
- [5] Alexey Dosovitskiy, Lucas Beyer, Alexander Kolesnikov, Dirk Weissenborn, Xiuhua Zhai, Thomas Unterthiner, Mostafa Dehghani, Matthias Minderer, Georg Heigold, Sylvain Gelly, Jakob Uszkoreit, and Neil Houlsby. 2020. An Image is Worth 16x16 Words: Transformers for Image Recognition at Scale. *CoRR* abs/2010.11929 (2020). arXiv:2010.11929 <https://arxiv.org/abs/2010.11929>
- [6] Gabriel Goh, Nick Cammarata †, Chelsea Voss †, Shan Carter, Michael Petrov, Ludwig Schubert, Alec Radford, and Chris Olah. 2021. Multimodal Neurons in Artificial Neural Networks. *Distill* (2021). <https://doi.org/10.23915/distill.00030> <https://distill.pub/2021/multimodal-neurons>.
- [7] Agrim Gupta, Piotr Dollar, and Ross Girshick. 2019. LVIS: A dataset for large vocabulary instance segmentation. In *Proceedings of the IEEE/CVF conference on computer vision and pattern recognition*. 5356–5364.
- [8] Chao Jia, Yunfei Yang, Ye Xia, Yi-Ting Chen, Zarana Parekh, Hieu Pham, Quoc V. Le, Yunhsuan Sung, Zhen Li, and Tom Duerig. [n. d.]. Scaling Up Visual and Vision-Language Representation Learning With Noisy Text Supervision. ([n. d.]). arXiv:2102.05918 <http://arxiv.org/abs/2102.05918>
- [9] Justin Johnson, Bharath Hariharan, Laurens Van Der Maaten, Li Fei-Fei, C Lawrence Zitnick, and Ross Girshick. 2017. Clevr: A diagnostic dataset for compositional language and elementary visual reasoning. In *Proceedings of the IEEE conference on computer vision and pattern recognition*. 2901–2910.
- [10] Aishwarya Kamath, Mannat Singh, Yann LeCun, Gabriel Synnaeve, Ishan Misra, and Nicolas Carion. [n. d.]. MDETR – Modulated Detection for End-to-End Multimodal Understanding. ([n. d.]). arXiv:2104.12763 <http://arxiv.org/abs/2104.12763>
- [11] Wonjae Kim, Bokyung Son, and Ildoo Kim. [n. d.]. ViLT: Vision-and-Language Transformer Without Convolution or Region Supervision. ([n. d.]). arXiv:2102.03334 <http://arxiv.org/abs/2102.03334>
- [12] Ranjay Krishna, Yuke Zhu, Oliver Groth, Justin Johnson, Kenji Hata, Joshua Kravitz, Stephanie Chen, Yannis Kalantidis, Li-Jia Li, David A Shamma, et al. 2017. Visual genome: Connecting language and vision using crowdsourced dense image annotations. *International journal of computer vision* 123, 1 (2017), 32–73.
- [13] Junnan Li, Dongxu Li, Silvio Savarese, and Steven Hoi. 2023. BLIP-2: Bootstrapping Language-Image Pre-training with Frozen Image Encoders and Large Language Models. arXiv:2301.12597 [cs.CV]
- [14] Liunian Harold Li, Mark Yatskar, Da Yin, Cho-Jui Hsieh, and Kai-Wei Chang. [n. d.]. VisualBERT: A Simple and Performant Baseline for Vision and Language. ([n. d.]). arXiv:1908.03557 <http://arxiv.org/abs/1908.03557>
- [15] Liunian Harold Li\*, Pengchuan Zhang\*, Haotian Zhang\*, Jianwei Yang, Chunyuan Li, Yiwu Zhong, Lijuan Wang, Lu Yuan, Lei Zhang, Jenq-Neng Hwang, Kai-Wei Chang, and Jianfeng Gao. 2022. Grounded Language-Image Pre-training. In *CVPR*.
- [16] Yangguang Li, Feng Liang, Lichen Zhao, Yufeng Cui, Wanli Ouyang, Jing Shao, Fengwei Yu, and Junjie Yan. 2021. Supervision exists everywhere: A data efficient contrastive language-image pre-training paradigm. *arXiv preprint arXiv:2110.05208* (2021).
- [17] Tsung-Yi Lin, Michael Maire, Serge Belongie, James Hays, Pietro Perona, Deva Ramanan, Piotr Dollár, and C Lawrence Zitnick. 2014. Microsoft coco: Common objects in context. In *European conference on computer vision*. Springer, 740–755.
- [18] Norman Mu, Alexander Kirillov, David A. Wagner, and Saining Xie. 2021. SLIP: Self-supervision meets Language-Image Pre-training. *CoRR* abs/2112.12750 (2021). arXiv:2112.12750 <https://arxiv.org/abs/2112.12750>
- [19] Michal Nazarczuk and Krystian Mikolajczyk. 2020. SHOP-VRB: A Visual Reasoning Benchmark for Object Perception. *International Conference on Robotics and Automation (ICRA)* (2020).
- [20] Alec Radford, Jong Wook Kim, Chris Hallacy, Aditya Ramesh, Gabriel Goh, Sandhini Agarwal, Girish Sastry, Amanda Askell, Pamela Mishkin, Jack Clark, Gretchen Krueger, and Ilya Sutskever. [n. d.]. Learning Transferable Visual Models From Natural Language Supervision. ([n. d.]). arXiv:2103.00020 <http://arxiv.org/abs/2103.00020>
- [21] Aditya Ramesh, Mikhail Pavlov, Gabriel Goh, Scott Gray, Chelsea Voss, Alec Radford, Mark Chen, and Ilya Sutskever. [n. d.]. Zero-Shot Text-to-Image Generation. ([n. d.]). arXiv:2102.12092 <http://arxiv.org/abs/2102.12092>
- [22] Olga Russakovsky, Jia Deng, Hao Su, Jonathan Krause, Sanjeev Satheesh, Sean Ma, Zhiheng Huang, Andrej Karpathy, Aditya Khosla, Michael S. Bernstein, Alexander C. Berg, and Li Fei-Fei. 2014. ImageNet Large Scale Visual Recognition Challenge. *CoRR* abs/1409.0575 (2014). arXiv:1409.0575 <http://arxiv.org/abs/1409.0575>
- [23] Konstantin Schall, Kai Uwe Barthel, Nico Hezel, and Klaus Jung. 2021. GPR1200: A Benchmark for General-Purpose Content-Based Image Retrieval. *CoRR* abs/2111.13122 (2021). arXiv:2111.13122 <https://arxiv.org/abs/2111.13122>
- [24] vijishmadhavan. 2022. Crop-CLIP. <https://github.com/vijishmadhavan/Crop-CLIP#Simple-App>.
- [25] Chenyun Wu, Zhe Lin, Scott Cohen, Trung Bui, and Subhransu Maji. [n. d.]. PhraseCut: Language-based Image Segmentation in the Wild. ([n. d.]). arXiv:2008.01187 <http://arxiv.org/abs/2008.01187>
- [26] Jiarui Xu, Shalini De Mello, Sifei Liu, Wonmin Byeon, Thomas Breuel, Jan Kautz, and Xiaoqiang Wang. 2022. GroupViT: Semantic Segmentation Emerges from Text Supervision. *arXiv preprint arXiv:2202.11094* (2022).
- [27] Lewei Yao, Runhui Huang, Lu Hou, Guansong Lu, Minzhe Niu, Hang Xu, Xiaodan Liang, Zhenguang Li, Xin Jiang, and Chunjing Xu. 2021. FILIP: Fine-grained Interactive Language-Image Pre-Training. *arXiv preprint arXiv:2111.07783* (2021).
- [28] Lu Yuan, Dongdong Chen, Yi-Ling Chen, Noel Codella, Xiyang Dai, Jianfeng Gao, Houdong Hu, Xuedong Huang, Boxin Li, Chunyuan Li, Ce Liu, Mengchen Liu, Zicheng Liu, Yumao Lu, Yu Shi, Lijuan Wang, Jianfeng Wang, Bin Xiao, Zhen Xiao, Jianwei Yang, Michael Zeng, Luowei Zhou, and Pengchuan Zhang. [n. d.]. Florence: A New Foundation Model for Computer Vision. ([n. d.]). arXiv:2111.11432 <http://arxiv.org/abs/2111.11432>
- [29] Yiwu Zhong, Jianwei Yang, Pengchuan Zhang, Chunyuan Li, Noel Codella, Liunian Harold Li, Luowei Zhou, Xiyang Dai, Lu Yuan, Yin Li, and Jianfeng Gao. 2021. RegionCLIP: Region-based Language-Image Pretraining. *CoRR* abs/2112.09106 (2021). arXiv:2112.09106 <https://arxiv.org/abs/2112.09106>
- [30] Kaiyang Zhou, Jingkang Yang, Chen Change Loy, and Ziwei Liu. 2021. Learning to prompt for vision-language models. *arXiv preprint arXiv:2109.01134* (2021).

## A APPENDIX

### A.1 The Effectiveness of Complete Cover

Let us explore the computational complexity of the number of all possible patches using a brute force algorithm. For an image with a side length of  $a$ , the total number of possible patches is  $O(a^4)$ , as each rectangular patch can be defined by its top-left and bottom-right corner coordinates. When limiting the patches to be square, the complexity remains significant at  $O(a^3)$ .

To simplify our analysis, we focus on square patches. In our main paper, we define  $c$  as the ratio of the perimeter, which is equivalent to the ratio of the side length. By adopting the Complete Cover scheme, we can generate patches at different levels with side lengths of  $[c, 2c, 3c, \dots, a]$ . For each level, the number of patches to cover all targets for corresponding sidelength are  $O((\frac{a}{c})^2)$ ,  $O((\frac{a}{2c})^2)$ ,  $O((\frac{a}{3c})^2)$ ,  $\dots$ ,  $O((\frac{a}{a})^2)$  respectively.

The total number of patches introduces by Complete Cover is:

$$\left(\frac{a}{c}\right)^2 * \left(1 + \frac{1}{2^2} + \frac{1}{3^2} + \dots\right) \quad (9)$$

$$= \left(\frac{a}{c}\right)^2 \times \frac{\pi^2}{6} \quad (10)$$

$$= O(a^2) \quad (11)$$

where  $c$  is a constant across the experiment.

In Figure 9, we illustrate the number of patches for various side lengths when  $c = 3$ , alongside a quadratic function  $y = 0.25x^2$ . The close fit between these two curves highlights the effectiveness of our approach.

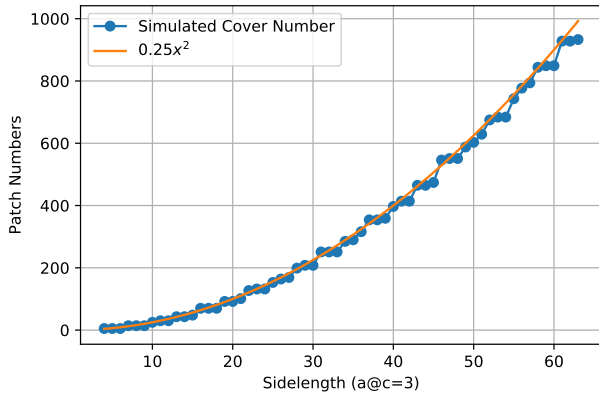


Figure 9: Patch numbers for different sidelengths when  $c = 3$ .

It is essential to note that before cropping patches, we resize the image to ensure the side length  $a$  is divisible by  $c$ . The minimum effective range for  $Q$  is determined as the range of side lengths for  $P$  that results in  $C(P, Q) = 1$ . We present the formulas for cover side length, minimum effective range, and the patch number for a given  $c$  in Table 7.

Table 7: Relationship between the cover sidelength, the minimum effective range, and the number of patches at a given  $c$

Level	Cover Sidelength	Minimum Effective Range	Patch Numbers
1	$a$	$a \geq x \geq \frac{a}{c}$	1
2	$a - c$	$\frac{a}{c} > x \geq \frac{a-c}{c}$	$\left(\frac{2c+ac-a}{-c^2+2c+ac-a}\right)^2$
3	$a - 2c$	$\frac{a-c}{c} > x \geq \frac{a-2c}{c}$	$\left(\frac{3c+ac-a}{-2c^2+3c+ac-a}\right)^2$
...	...	...	...
n	$\left(\frac{nc+ac-a}{-(n-1)c^2+nc+ac-a}\right)^2$	$\frac{a-(n-2)c}{c} > x \geq \frac{a-(n-1)c}{c}$	$a - (n-1)c$
...	...	...	...

Table 8: Statistics of CLEVR-DS

Per Image	Mean	Min	Max
Instance	13.78	1	50
Class	13.78	1	50

Table 9: Statistics of MSCOCO

Per Image	Mean	Min	Max
Instance	7.33	1	93
Class	2.92	1	18

Table 10: Statistics of Unity-Retail

Per Image	Mean	Min	Max
Instance	25.52	16	42
Class	13.52	9	19

### A.2 Data Statistics

We have selected several datasets for performing the class with prompt text-to-image retrieval tasks. The statistics for CLEVR-DS, Unity-Retail, MSCOCO, and LVIS can be found in Table 8 through Table 12. These four datasets contain relatively more instances per image compared to other datasets, increasing the likelihood of small objects within the images. Notably, the mean number of instances per image for CLEVR-DS is higher than that of LVIS. A demo for CLEVR-DS dataset is shown in Figure 10.

### A.3 More Ablation study

To thoroughly evaluate our method’s retrieval capabilities, we utilize a smaller CLEVR-DS dataset containing an average of three objects per image without any occlusion. The subsequent ablation studies employ this reduced dataset.

*A.3.1 DetailCLIP Performance Under Different Complete Cover Schemes.* We present the number of patches at different levels based on varying  $c$  values in Table 13. For notational convenience, we set  $\frac{a}{c} = k$ .

**Table 11: Statistics of LVIS**

Per Image	Mean	Min	Max
Instance	11.2	1	294
Class	3.4	1	24

**Table 12: Class number of datasets.**

DATASET	COCO	LVIS	CLEVR-DS	Unity-Retail
Image Number	122,219	122,219	10,000	1,000
Class Number	80	1230	138	16

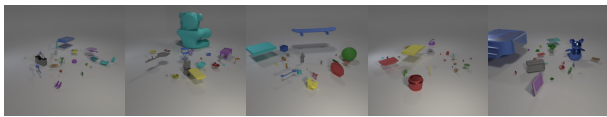


**Figure 10: Our synthetic CLEVR-DS dataset illustrated above, is similar to the original CLEVR dataset but presents more complex scenes. We randomly scatter 1-50 instances from 138 ShapeNet object classes within each image. These images feature 1-3 large objects and more than 10 small objects, significantly increasing the challenge for the text-to-image retrieval task.**

**Table 13: Number of patches at different levels.**

CC@k	Patch Numbers	Level 1	Level 2	Level 3	Level 4	Level 5	Level 6	Level 7
1	1	1						
2	5	1	4					
3	14	1	4	9				
4	30	1	4	9	16			
5	39	1	4	9	25			
6	66	1	4	9	16	36		
7	79	1	4	9	16	49		
8	103	1	4	9	25	64		
9	136	1	4	9	16	25	81	
10	166	1	4	9	16	36	100	
11	187	1	4	9	16	36	121	
12	248	1	4	9	16	25	49	144
13	273	1	4	9	16	25	49	169
14	315	1	4	9	16	25	64	196
15	355	1	4	9	16	36	64	225

To determine an appropriate  $k$ , we examine the performance of the DetailCLIP model across 14 distinct  $k$  values. The results are displayed in Figure 11. Lines with star markers represent retrieval results, while those without indicate DetailCLIP results. Dashed lines correspond to recall@1 results, and the same color is used for the same patch selection method under identical recall metrics. The figure reveals several observations:

- The recall@1 results for DetailCLIP (single feature) are on par with the retrieval baseline (multi-feature) for any  $k$ . DetailCLIP performs marginally better with larger  $k$  values.
- The performance of both DetailCLIP and the retrieval baseline starts to increase at  $k = 2$  and plateaus at  $k = 9$ . For recall@1, patch-cc outperforms patch-grid beginning at  $k = 4$ .

- For  $k \geq 8$ , the number of patches grows significantly, but the performance of the DetailCLIP model does not.

Based on the above analysis and considering the trade-off between DetailCLIP performance and computational complexity, we opt for  $k = 10$  for the experiments presented in the main body of our paper. Notably, when  $k = 10$ , the last level of patch number aligns with the patch-grid method.

#### A.4 Hyper-parameter Tuning

For training DetailCLIP, we employ the AdamW optimizer, a linear learning rate scheduler, and a linear warm-up training strategy over 10 epochs. DetailCLIP is trained using a single GTX 2080ti, with a batch size of 30 across all experiments.

For different  $k$  values, we independently perform a grid search of DetailCLIP hyperparameters, as shown in the table below. We select the optimal hyperparameters on a validation set and report the results on a held-out test set.

**Table 14: Hyper-Parameter candidate in validation Set.**

Name	Candidate
Learning Rate	[0.001, 0.003, 0.005, 0.007, 0.01]
Weight Decay	[0, 0.001]
Step Size for Learning Rate Decay	[60, 120]
Gamma Value for Learning Rate Decay	[0.5, 0.7, 0.9]
Gradient Clip Value	[0.00001, 0.0001]
Layer Normalization's Epsilon	[0.0001, 0.001, 0.01]

#### A.5 Pytorch-Like Code

A Pytorch style code and the complete pipeline of our DetailCLIP model are listed in Listing 1.

```

1 from einops import rearrange
2
3
4 def compute_loss(fusing_model, patch_feature,
5                 vanilla_feature, text_feature):
6     # b: batch size
7     # p: number of patch
8     # t: number of text feature
9     # f: feature dim
10    # vanilla_feature: clip feature for entire image, (b, f)
11    # patch_feature: clip feature for different patches, (b, p, f)
12    # text_feature: clip feature for text prompts, (t, f)
13    # fusing_model: DetailCLIP model
14    # All features are normalized.
15    DetailCLIP_feature = fusing_model(patch_feature,
16    vanilla_feature)
17    patch_feature = rearrange(patch_feature, 'b p f -> (b p) f')
18    proxy_feature = text_feature
19    # (t, f) @ (f, b * p) -> (t, b * p)
20    q_p_similarity = proxy_feature @ patch_feature.T
21    q_p_similarity = rearrange(q_p_similarity, 'k (b p) -> k b p')
22    # (t, b, p) -> (t, b)
23    q_p_similarity_max = q_p_similarity.max(-1)
24    # (t, f) @ (f, b) -> (t, b)
25    q_c_similarity = proxy_feature @ DetailCLIP_feature.T

```

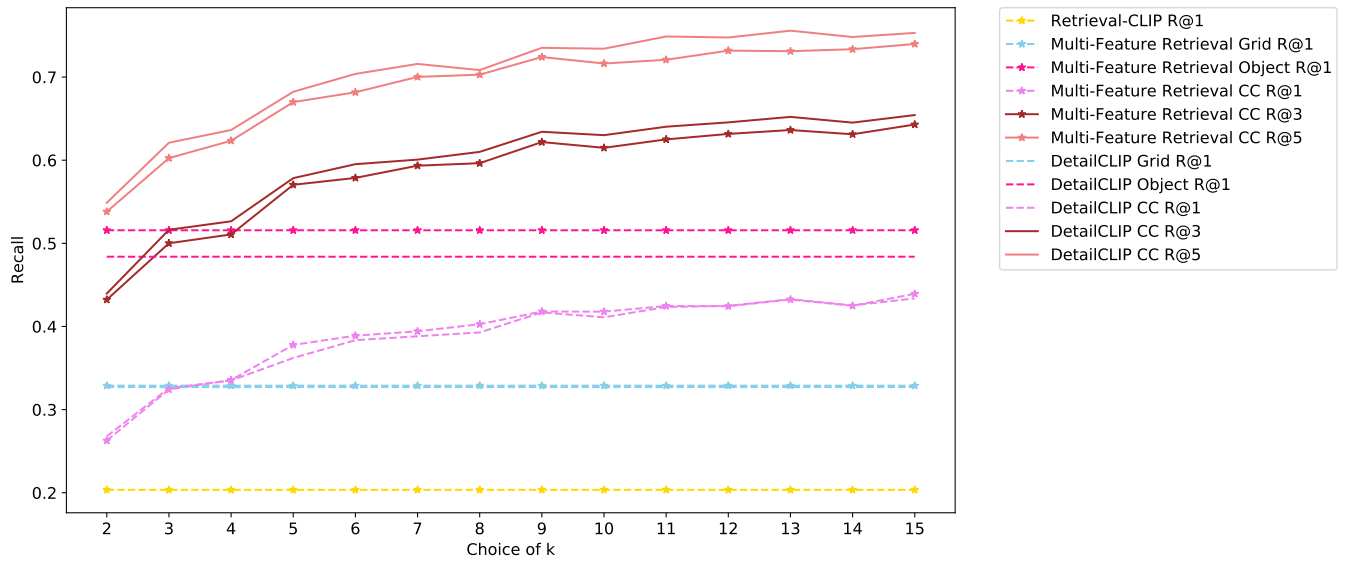


Figure 11: Recall for retrieval and DetailCLIP models with different  $k$  Values

```

24 query_proxy_loss = mse_loss(q_p_similarity_max,
    q_c_similarity)
    
```

Listing 1: Pytorch-Like Code

## A.6 Retrieval Result Visualization

Query	Model	Retrieval Index Top 1 - 10									
Airplane	CLIP										
	Detail CLIP										
Calculator	CLIP										
	Detail CLIP										
Fruit	CLIP										
	Detail CLIP										
Bear	CLIP										
	Detail CLIP										
USBStick	CLIP										
	Detail CLIP										

Figure 12: Retrieval Result Visualization: Ground truth images for each query are highlighted with blue frames, while other images are surrounded by green frames. Please note that two rows make up a group, with each row representing a ranked retrieval result – the higher the proportion of blue frames, the better the performance. The upper row in each group displays the top 10 retrieval results for CLIP, while the lower row shows the results for DetailCLIP. Ground truth objects are marked with red bounding boxes for visualization purposes. It is important to note that neither of the methods presented here generates bounding boxes.